2130–2143 *Nucleic Acids Research, 2011, Vol. 39, No. 6* *Published online 12 November 2010*
doi:10.1093/nar/gkq1095

Mismatch-repair protein MSH6 is associated with Ku70 and regulates DNA double-strand break repair

Ankita Shahi[1,2], Jung-Hee Lee[1,3], Yoonsung Kang[1,3], Sung Haeng Lee[4], Jin-Won Hyun[5], In-Youb Chang[1,6], Jae-Yeoul Jun[1,7] and Ho Jin You[1,2,*]

[1]DNA Repair Research Center, [2]Department of Pharmacology, [3]Department of Biometerials, [4]Department of Cellular and Molecular Medicine, Chosun University School of Medicine, 375 Seosuk-dong, Gwangju, 501-759, South Korea, [5]Department of Biochemistry, College of Medicine Cheju National University, Jeju. Jeju-do, Korea, [6]Department of Anatomy, [7]Department of Physiology, Chosun University School of Medicine, 375 Seosuk-dong, Gwangju, 501-759, South Korea

Received May 17, 2010; Revised October 13, 2010; Accepted October 15, 2010

ABSTRACT

MSH6, a key component of the MSH2–MSH6 complex, plays a fundamental role in the repair of mismatched DNA bases. Herein, we report that MSH6 is a novel Ku70-interacting protein identified by yeast two-hybrid screening. Ku70 and Ku86 are two key regulatory subunits of the DNA-dependent protein kinase, which plays an essential role in repair of DNA double-strand breaks (DSBs) through the non-homologous end-joining (NEHJ) pathway. We found that association of Ku70 with MSH6 is enhanced in response to treatment with the radiomimetic drug neocarzinostatin (NCS) or ionizing radiation (IR), a potent inducer of DSBs. Furthermore, MSH6 exhibited diffuse nuclear staining in the majority of untreated cells and forms discrete nuclear foci after NCS or IR treatment. MSH6 colocalizes with γ-H2AX at sites of DNA damage after NCS or IR treatment. Cells depleted of MSH6 accumulate high levels of persistent DSBs, as detected by formation of γ-H2AX foci and by the comet assay. Moreover, MSH6-deficient cells were also shown to exhibit impaired NHEJ, which could be rescued by MSH6 overexpression. MSH6-deficient cells were hypersensitive to NCS- or IR-induced cell death, as revealed by a clonogenic cell-survival assay. These results suggest a potential role for MSH6 in DSB repair through upregulation of NHEJ by association with Ku70.

INTRODUCTION

DNA double-strand breaks (DSBs) are considered to be the most biologically damaging lesions produced by ionizing radiation (IR) and certain chemicals (1). DSBs are more prone to unsuccessful or inaccurate DNA repair due to the lack of a complementary template. Unrepaired DNA damage can lead to cell-cycle arrest and apoptosis, while accumulation of inaccurate repairs can lead to chromosomal instability and carcinogenesis (2). Homologous recombination (HR) and non-homologous end-joining (NHEJ) are the two principal pathways that mediate repair of DSBs in eukaryotic cells (1,3). HR utilizes the homologous sister chromatid or homologous chromosome as a template, resulting in error-free repair of the missing information in the damaged DNA. In contrast, NHEJ is referred to as an intrinsically error-prone-repair pathway because this process joins the two broken-DNA ends without using a homologous template. In NHEJ, bases are generally deleted or inserted as a part of repair of the DSB. Despite the mutagenic nature of NHEJ, this pathway is responsible for repairing a major fraction of DNA DSBs in higher eukaryotes.

NHEJ is a complex process, requiring many protein components. To initiate NHEJ, Ku70 binds the broken DNA ends as a ring-shaped heterodimer complex together with Ku86 (4). The Ku complex binds free ends without any sequence specificity, leading to recruitment of the catalytic subunit of the DNA-dependent protein kinase (DNA-PK_{CS}), a member of the phosphatidylinositol 3-kinase family. Together, Ku70, Ku86 and DNA-PK_{CS} form the active DNA–PK complex.

*To whom correspondence should be addressed. Tel: +82 62 230 6337; Fax: +82 62 230 6586; Email: hjyou@chosun.ac.kr

The authors wish it to be known that, in their opinion, the first two authors should be regarded as joint First Authors.

Assembly of this trimeric complex on the ends of double-stranded DNA activates the kinase activity of DNA-PK_{CS}. Subsequently, ligase IV and its cofactor, XRCC4, are recruited to perform ligation of the free DNA ends (4–6). Thus, DNA-PK_{CS} and Ku70 are essential for the initiation of NHEJ repair and are rate-limiting.

The Ku proteins were originally identified as autoantigens in patients with scleroderma polymyositis syndrome (7). Ku70 is made up of 609 amino acids, generating a 70-kDa protein, and forms a heterodimer with the 80-kDa Ku86 subunit (also known as Ku80), which consists of 732 amino acids. Both Ku proteins have an intrinsic nuclear localization signal and primarily localize to the nucleus (8). Ku70 and Ku86 show only 14% homology to one another. However, structural analysis of the two proteins bound to double-stranded DNA has shown that the two proteins are structurally similar, despite the lack of sequence homology.

Ku proteins are multifunctional proteins that possess deubiquitylation activity and play a key role in DNA repair and transcriptional regulation (9–12). Substantial biochemical evidence also indicates that various proteins physically interact with the Ku complex. For example, Ku70/80 interacts with both the protein and RNA components of human telomerase, suggesting that the Ku complex is involved in telomere maintenance in higher eukaryotes (13,14). The Ku complex has been shown to inhibit apoptosis through an association with the proapoptotic factor Bax (15). Interactions between Ku70 and p18-cyclin E, and Ku70 and Bax, provide a balance between apoptosis and cell survival in response to genotoxic stress (16). Ku70 interacts with Runx3 in the nucleus, suggesting a possible link between a tumor suppressor function and DNA repair (17). The human Werner-syndrome protein (WRN), which is a member of the RecQ helicase family, also interacts with Ku70/80, and these proteins are thought to serve a function in one or more pathways of DNA metabolism (18,19). The Ku70/80 complex also binds RAG1, providing a biochemical link between the two phases of V(D)J recombination. Furthermore, the cell polarity protein Par3 plays a role in efficient repair of DSBs through association with the DNA–PK complex (20).

In this study, we report that Ku70 associates physically with the mismatch repair (MMR) protein MSH6. MMR is a highly conserved DNA-repair pathway, and defective MMR is strongly associated with hereditary non-polyposis colorectal cancer (HNPCC) (21). In addition to a role in correcting mismatches formed during replication, MMR has recently been implicated in DSB repair after exposure to γ-irradiation (22–25). Our results indicate that MSH6-deficient cells have a major DSB-repair defect, shown by both the presence of γ-H2AX foci and by comet-tail analysis. Further biochemical analyses show that MSH6 knockdown or overexpression leads to downregulation or upregulation of NHEJ, respectively. These results suggest that MSH6 is involved in the repair of DSBs through a direct physical interaction with Ku70.

MATERIALS AND METHODS

Cell culture and drug treatment

The human cervix adenocarcinoma cell line HeLa and the human embryonic kidney cell line HEK293T were cultured in Dulbecco's modified Eagle's medium (Gibco-BRL, Grand Island, NY, USA). The DLD1 colon cancer cell line was cultured in RPMI-1640 medium (Gibco-BRL). In both cases, the media was supplemented with 10% heat-inactivated fetal bovine serum (Cambrex Corp., East Rutherford, NJ, USA), 100 units/ml penicillin, and 100 μg/ml streptomycin sulfate (Invitrogen, Carlsbad, CA, USA). All cells were maintained in a humidified incubator containing 5% CO_2 at 37°C. HeLa and DLD1 cell lines were obtained from the American Type Culture Collection (ATCC, Rockville, MD, USA), and the HEK293T cell line was obtained from the Cornell Institute for Medical Research (New York, NY, USA). To induce DNA breaks, exponentially growing cells were treated with the radiomimetic drug neocarzinostatin (NCS; Sigma, St Louis, MO, USA) at a final concentration of 100 ng/ml in fresh cell media or irradiated at 5 Gray (Gy) from ^{137}Cs source (Gammacell 3000 Elan irradiator, Best Theratronics, Ottawa, Canada) and allowed to recover at 37°C for various amounts of time.

Generation of stable MSH6 knockdown clones

The pSilencer2.1–U6 neo vector were obtained from Ambion (Austin, TX, USA). Vectors for expression of hairpin siRNAs were constructed by inserting corresponding pairs of annealed DNA oligonucleotides into the pSilencer 2.1–U6 vector between the *Bam*HI and *Hin*dIII restriction sites according to the manufacturer's instructions. The MSH6-specific target sequence was selected based on an online shRNA application from Invitrogen (http://www.ambion.com/techlib/nisc/psilencer-converter.html) using the human MSH6 sequence as the reference sequence (GenBank Accession No. NM_000179.2). The target sequences were 5′-GCCAGACACUAAGGAGGAA dTdT-3′ (sense) and 5′-UUCCUCCUUAGUGUCUGGC dTdT-3′ (antisense) for MSH6 siRNA #1 and 5′-GCGACUGUUCUAUAACUUU dTdT-3′ (sense) and 5′-AAAGUUAUAGAACAGUCGCdTdT-3′ (antisense) for MSH6 siRNA #2. A non-targeting sequence, 5′-CCUACGCCACCAAUUUCGU dTdT-3′ and 5′-ACGAAAUUGGUGGCGUAGG dTdT-3′, was used as a negative control. To generate single knockdown clones, HeLa cells were transfected with pSilencer2.1–U6, pSilencer2.1–U6 MSH6 siRNA #1 or pSilencer2.1–U6 MSH6 siRNA #2. Twenty-four hours after transfection, 400 μg/ml G418 was added to the culture medium for selection. After selection, stable clones were analyzed by real-time RT-PCR and western blotting to confirm downregulation of MSH6.

Plasmid constructs

The full-length Ku70 cDNA was amplified from GM00637 human fibroblast cells by RT-PCR using the Ku70 primers 5′-AATCTCGAGATGTCAGGGTGGGAG-3′ (sense) and 5′-AATGGGCCCTCAGTCCTGGA

AGTG-3′ (antisense). The amplified Ku70 cDNA construct was cloned into the mammalian expression vector pcDNA3 in-frame with the hemagglutinin (HA) tag. The Ku70 sequence was confirmed by automated DNA sequencing. The human MSH6 expression vector and its control vector were obtained from Origene (OriGene Technologies, Inc., Rockville, MD, USA).

Antibodies

The following antibodies were used for immunoblotting: mouse monoclonal anti-MSH6 (1:2000 BD Transduction Laboratories, Franklin Lakes, NJ, USA), mouse monoclonal anti-MSH2 (1:2000; Calbiochem, San Diego, CA, USA), monoclonal anti-Ku70 (1:2000; BD Transduction Laboratories), monoclonal anti-XRCC4 (BD Transduction Laboratories), monoclonal anti-DNA-PK_{CS} (1:2000; Santa Cruz Biotechnology, Santa Cruz, CA, USA), polyclonal anti-Ku86 (1:2000; Santa Cruz Biotechnology), monoclonal anti-HA tag (1:2000; Santa Cruz Biotechnology) and monoclonal anti-α-tubulin (1:8000; Neomarkers, Fremont, CA, USA). MSH6 foci were detected by immunofluorescence staining using the MSH6 antibody (H-141; Santa Cruz Biotechnology) at a 1:50 dilution. γ-H2AX foci were detected by immunofluorescence staining using the γ-H2AX mouse monoclonal antibody (JBW301, Upstate Biotechnology, Temecula, CA, USA) at a 1:200 dilution. Immunoprecipitations of endogenous and exogenous proteins were performed using rabbit polyclonal antibodies directed against MSH6 (ab50604; Abcam, Cambridge, UK) and Ku70 (H-308; Santa Cruz Biotechnology).

Yeast two-hybrid analysis

The full-length Ku70 was sub-cloned into pGBT9 vector, which expresses proteins fused to the GAL4-DNA-binding domain (DNA-BD) (Clontech, Mountain View, CA, USA). This vector was used as bait to screen a human prostate cDNA library fused to the GAL4 activation domain according to the manufacturer's (Clontech) instructions. Positive clones were verified by ono-on-one transformation and selection on agar plates lacking leucine and tryptophan (-LH) or adenine, histidine, leucine and tryptophan (-AHLT) and also processes for a β-galactosidase assay.

Immunoprecipitation assay and western-blot analysis

Cells were lysed in ice-cold NP-40 lysis buffer [50 mM Tris–HCl (pH 8.0), 150 mM NaCl, 1% Nonidet P-40] containing ethylenediaminetetraacetic acid (EDTA)-free protease inhibitor cocktail (Roche, Basel, Switzerland). Equal amounts of proteins were then resolved on 6–15% SDS-PAGE gels, followed by electrotransfer to polyvinylidene difluoride membranes (Millipore, Bedford, MA, USA). The membranes were blocked for 2 h in TBS-t [10 mM Tris–HCl (pH 7.4), 150 mM NaCl, 0.1% Tween 20] containing 5% fat-free milk at room temperature and then incubated with the indicated primary antibodies overnight at 4°C. After incubation for 2 h with appropriate peroxidase conjugated secondary antibodies, developed using enhanced chemiluminescence detection system.

For the immunoprecipitation assay, aliquots of soluble cell lysates were precleared with protein A/G plus- agarose beads (Santa Cruz Biotechnology), G sepharose and A sepharose (GE Healthcare) as indicated and then incubated at 4°C for 3 h. If DNase1 or ethidium bromide was used, the whole cell lysates were either treated with 100 μg/ml DNase1 (Invitrogen) for 20 min at 37°C or 50 μg/ml ethidium bromide (Sigma) on ice for 30 min. Next, the appropriate antibody was added, and incubated at 4°C for 12 h. After the addition of fresh protein A/G plus-agarose bead, G sepharose and A sepharose, the reaction was incubated overnight at 4°C with rotation. The beads were washed five times in RIPA buffer without protease inhibitors, resuspended in SDS sample buffer and boiled for 5 min. The samples were then analyzed by western blotting using the appropriate antibodies.

Immunostaining

To visualize γ-ray- or NCS-induced foci, untreated cells or cells treated with 100 ng/ml NCS were cultured on coverslips coated with poly-L-lysine (Sigma). Cells were washed twice with PBS and fixed in 98% methanol for 10 min, followed by permeabilization with 0.3% Triton X-100 for 15 min at room temperature. Next, the coverslips were washed three times with PBS, followed by blocking with 0.1% bovine serum albumin in PBS for 1 h at room temperature. The cells were double-immunostained using primary antibodies directed against the indicated proteins overnight at 4°C. The cells were then washed with PBS and stained with the appropriate Alexa Fluor 488- or Alexa Fluor 594-conjugated secondary antibodies (green and red fluorescence, respectively; Molecular Probes, Eugene, OR, USA). After washing, the coverslips were mounted onto slides using Vectashield mounting medium containing 4,6-diamidino-2-phenylindole (DAPI; Vector Laboratories, Burlingame, CA, USA). Fluorescence images were taken under a confocal microscope (Zeiss LSM 510 Meta; Carl Zeiss, Jena, Germany) and analyzed with Zeiss LSM Image Examiner software (Carl Zeiss). For foci quantification experiments, cells with $\geq$10 foci were counted as MSH6 or γ-H2AX foci-positive cells and the percentage was calculated among at least 100 cells by dividing the number of MSH6 or γ-H2AX foci-positive cells by the number of DAPI-stained cells. The error bars represent standard error in three independent experiments.

Cell survival assay

After treatment with NCS or IR, 5×10^2 cells were immediately seeded onto a 60-mm dish in duplicate and grown for 2–3 weeks at 37°C to allow colony formation. Colonies were stained with 2% methylene blue in 50% ethanol and counted. The fraction of surviving cells was calculated as the ratio of the plating efficiencies of treated cells to untreated cells. Cell survival results are reported as the mean value ± standard deviation for three independent experiments.

Comet assay

DSB repair was assayed by alkaline single-cell agarose-gel electrophoresis as described previously. Briefly, control and MSH6-knockdown cells were treated with 100 ng/ml NCS or 5 Gy of γ-ray by followed by incubation in culture medium at 37°C for the indicated times. Cells were then harvested (~10^5 cells per pellet), mixed with low-melting temperature agarose, and layered onto agarose-coated glass slides. The slides were maintained in the dark at 4°C for all of the remaining steps. Slides were submerged in lysis solution [10 mM Tris–HCl (pH 10), 2.5 M NaCl, 0.1 M EDTA, 1% Triton X-100, 10% dimethyl sulfoxide] for 1 h and incubated for 30 min in alkaline electrophoresis solution (300 mM NaOH, 200 mM EDTA at pH >13). After electrophoresis (~30 min at 1 V/cm tank length), air-dried and neutralized slides were stained with 30–50 μl ethidium bromide (20 μg/ml). Average comet tail moment was scored for 40–50 cells/slide using a computerized image analysis system (Komet 5.5; Andor Technology, South Windsor, CT, USA).

Analysis of NHEJ activity

To analyze the role of MSH6 in NHEJ *in vivo*, we used the pEGFP-Pem1-Ad2 system (26). The plasmid was digested with *Hin*dIII to remove Ad2 and generate different types of ends. Supercoiled pEGFP-Pem1 was used as a positive control for standardization of transfection and analysis conditions. The pCMV-dsRed-express plasmid (Clontech) was co-transfected with either linearized pEGFP-Pem1-Ad2 or supercoiled pEGFP-Pem1 as a control for transfection efficiency. In a typical reaction, 5×10^5 cells were transfected with 0.5 μg of linearized pEGFP-Pem1-Ad2 or 0.5 μg supercoiled pEGFP-Pem1, together with 0.5 μg of pDsRed2-N1 plasmid, using Lipofectamine 2000 (Invitrogen) according to the manufacturer's recommended protocol. Twenty-four hours after transfection, green (EGFP) and red (DsRed) fluorescence was measured by flow cytometry (FACSCalibur; BD Biosciences, San Jose, CA, USA).

Statistical analysis

Data are presented as means ± SD. Statistical comparisons were carried out using unpaired *t*-tests, and values of $P < 0.01$ were considered to be statistically significant.

RESULTS

Protein interaction studies of the human Ku70 with MSH6

A yeast two-hybrid screen of a human prostate cDNA library using full-length human Ku70 as bait was carried out to identify potential Ku70-binding proteins. One of the positive clones isolated from the 2×10^6 transformants was identified as human MSH6. To further confirm MSH6′s interaction with Ku70, we contransformed Ku70 constructs with MSH6. The transformed colonies showed the ability to grow in medium lacking adenosin, histidine, tryptophan and leucine (-AHLT) and to turn blue in a β-galactosidase assay, while cells contransformed with the control vector pGBT9 vector did not do so with a construct containing the human MSH6 cDNA (Supplementary Figure S1).

To determine whether Ku70 interacts with MSH6 in human cells endogenously expressing both proteins, we utilized immunoprecipitation assays. For production of DSBs, HeLa cells were treated with 100 ng/ml of the radiomimetic drug NCS or 5 Gy of IR. The cells were then lysed, and endogenous MSH6 was immunoprecipitated with a MSH6-specific antibody. Immunoprecipitates were subjected to western blotting with an anti-Ku70 antibody. Immunoprecipitation with anti-MSH6 antibodies revealed that endogenous MSH6 bound Ku70 and that treatment with NCS or IR increased the amount of MSH6 bound to Ku70 (Figure 1A). In this reciprocal experiments, Ku70 antibody was able to coimmunoprecipitate MSH6 (Figure 1B), suggesting that these proteins may interact with each other directly or indirectly in cells. As control, normal rabbit IgG did not coimmunoprecipitate Ku70 or MSH6, indicating that the coimmunoprecipitation of Ku70 with MSH6 was not due to non-specific antibody binding. Because the MSH6 protein is complexed with MSH2 to form the MutSα heterodimer (27), we tested whether Ku70 interacts with MSH2. When proteins were immunoprecipitated with anti-Ku70 and then probed with anti-MSH2, MSH2 was detected (Figure 1B, second panel).

To further document, the physiological relevance of the interaction, we investigated whether MSH6 interacts with other components of the NHEJ system by coimmunoprecipitation assays. NHEJ is initiated by binding of the Ku70/86 heterodimer to both ends of the broken DNA molecule, and this step is essential for recruitment of DNA-PK_{CS} (4). The assembled DNA-PKcs then exhibits serine-threonine protein kinase and DNA end-bridging activities (28). Finally, the XRCC4/DNA ligase IV complex is responsible for the ligation step (29,30). Endogenous MSH6 and Ku86 could be coimmunoprecipitated by anti-MSH6 antibodies (Figure 1C, second panel), but not by control IgGs, and this was increased after treatment of NCS. We then tested whether MSH6 binds DNA-PK_{CS} or XRCC4 in human cells. Immunoprecipitation of lysates using anti-MSH6 antibodies revealed that endogenous MSH6 and DNA-PKcs did not interact in the absence of NCS, but upon NCS treatment the interaction was found (Figure 1C, third panel). However, interaction between MSH6 and XRCC4 in the presence of NCS was not detected by coimmunoprecipitation (Figure 1C, fourth panel). Since both MSH6 and Ku70 are chromatin-bound proteins in cells, we considered the possibility that the interaction between MSH6 and Ku70 was mediated by the independent binding of both protein complexes to DNA. To exclude this possibility, we pretreated cell lysates with DNase I, or ethidium bromide (EtBr), which is known to disrupt protein–DNA interactions, prior to coimmunoprecipitation. Our data showed that DNA did not mediate MSH6-Ku70 association (Figure 1D). These results suggested that MSH6 forms a physiological complex with Ku heterodimer *in vivo*.

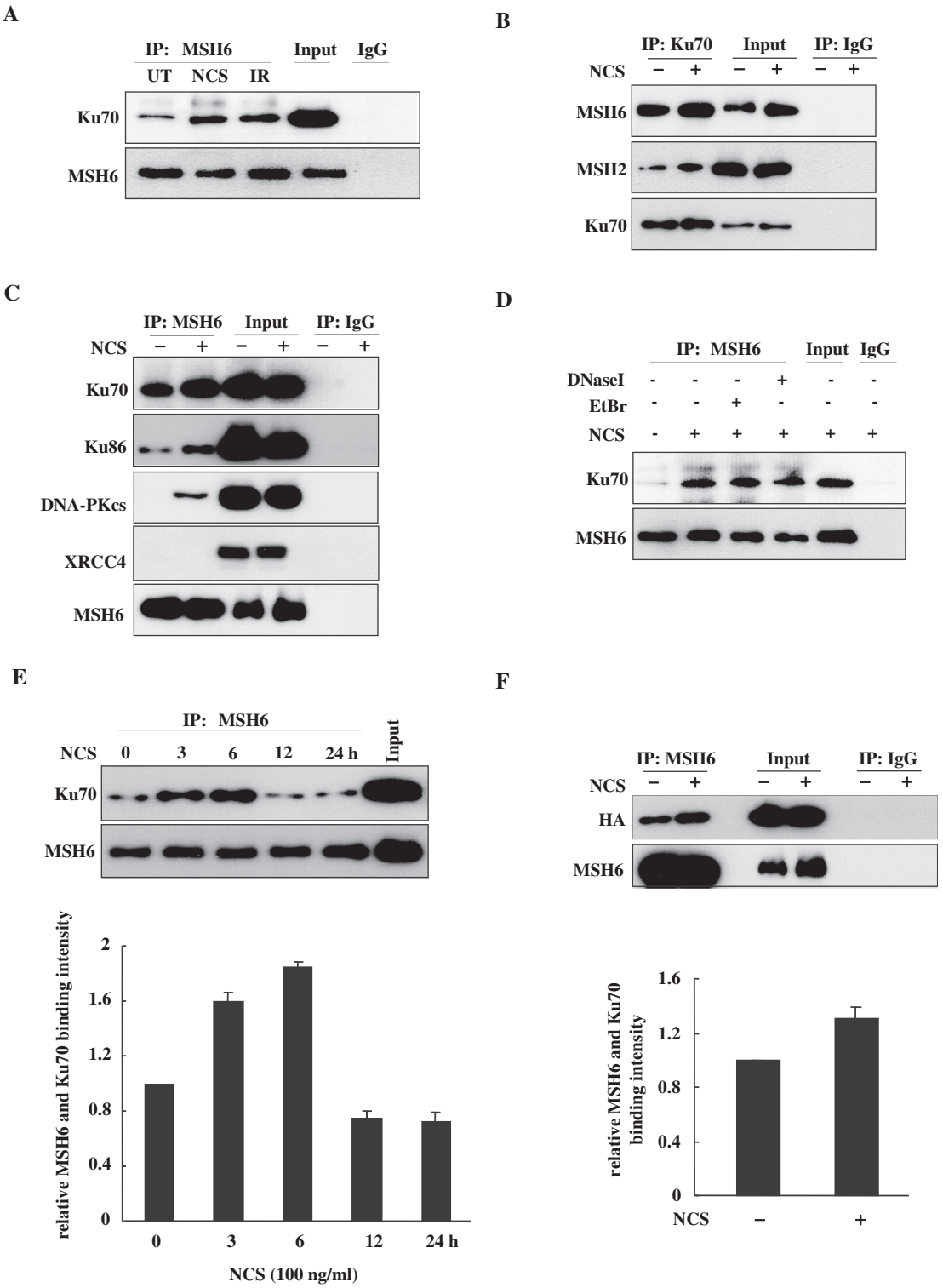

Figure 1. MSH6 interacts with Ku70. (**A**) HeLa cells were untreated (UT) or treated with 100 ng/ml NCS or 5 Gy ionizing radiation (IR). Proteins were immunoprecipitated (IP) from the lysates using an anti-MSH6 antibody 3 h after treatment. Immunoprecipitates were then subjected to western-blot analysis using antibodies specific for Ku70 or MSH6. The fourth lane contain 5% input for Ku70 and 20% input for MSH6. Normal rabbit IgG was used for negative control immunoprecipitations. (**B**) HeLa cells were untreated or treated with 100 ng/ml NCS for 3 h. Proteins were immunoprecipitated from the lysates using an anti-Ku70 antibody. Immunoprecipitates were then subjected to western-blot analysis using antibodies specific for MSH6, MSH2 or Ku70. The third and fourth lane contains 5% input for Ku70 and 20% input for MSH6 and MSH2. Normal rabbit IgG was used for negative control immunoprecipitations. (**C**) HeLa cells were untreated or treated with 100 ng/ml NCS for 3 h. Proteins were immunoprecipitated from the lysates using an anti-MSH6 antibody. Immunoprecipitates were then subjected to western-blot analysis using antibodies specific for Ku70, Ku86, DNA-PK$_{CS}$, XRCC4 or MSH6. The third and fourth lane contains 5% input for Ku70 and 20% input for Ku86, DNA-PKcs, XRCC4 and MSH6. Normal rabbit IgG was used for negative control immunoprecipitations. (**D**) HeLa cells were untreated or treated with 100 ng/ml NCS for 3 h. Whole cell lysates were treated with 50 μg/ml ethidium bromide (EtBr) on ice for 30 min (lane 3) or 100 μg/ml

Continued

We next investigated the binding kinetics of MSH6 and Ku70 at different time periods after treatment with NCS. Immunoprecipitation analysis revealed that the level of interaction between the two proteins clearly increased by 3 h after NCS treatment and further increased by 6 h after treatment, then decreased in a time-dependent manner (Figure 1E). These observations indicate that Ku70 and MSH6 complex formation increases at the early onset of DSB formation and dissociates at later time points.

To further confirm this interaction, HEK293T cells were transiently transfected with an expression construct encoding full-length Ku70 tagged with HA and a second construct that expressed full-length MSH6. Co-immunoprecipitation assays were then performed using an MSH6-specific antibody for immunoprecipitation and an anti-HA antibody for immunoblotting. Immunoprecipitation with the anti-MSH6 antibody revealed that MSH6 was associated with HA-tagged, full-length Ku70 in both control and NCS-treated cells and that the level of binding increased after NCS treatment (Figure 1F). Therefore, it is likely that MSH6 forms a complex with Ku70. In spite of this, it remains possible that other proteins may mediate the interaction between MSH6 and Ku70 complex because both complexes possess a variety of interacting partners.

MSH6 forms nuclear foci and colocalizes with γ-H2AX in response to DNA damage

After DNA damage, many DNA-damage-repair proteins are recruited to the DNA-damage sites and form discrete DNA-damage-induced nuclear foci. The order and timing of these events are thought to be critical for DNA repair (31). Thus, we were interested in whether MSH6 also forms NCS- or IR-induced nuclear foci. In untreated HeLa cells, anti-MSH6 antibody staining yielded diffuse nuclear staining (Figure 2A and B). Numerous nuclear foci were apparent in cells 1 h after 100 ng/ml NCS treatment (Figure 2A). MSH6 foci were also evident in HeLa cells 30 min after irradiation at 5 Gy (Figure 2B). MSH6 foci peak at 6 or 12 h after NCS or IR treatment, respectively, and then significantly declined. We also tested whether Ku70 could form nuclear foci after NCS treatment. However, Ku70 did not form nuclear foci. Ku70 staining in NCS- or IR-treated cells was weak and diffuse throughout the nucleus (data not shown).

γ-H2AX focus formation on the DSB sites is one of the earliest events in response to forms of DNA damage that induce DSBs (32). Based on above observations, we investigate the potential colocalization of MSH6 and γ-H2AX into the same nuclear foci after DNA damage. Thus, the immunofluorescent staining analysis was conducted. As shown in Figure 2C, MSH6 in the mock-treated cells appears to be homogenously distributed through the nucleus and γ-H2AX foci was not found. Upon NCS or IR treatment, a clear redistribution of MSH6 and γ-H2AX to form discrete nuclear foci occurred (Figure 2C and D). Some extent of colocalization of these foci occurred. Such limited degree of colocalization was probably reflecting the fact that both MSH6 and γ-H2AX are able to interact with several protein partners and function in multiple biological pathways in cells. A quantitative assessment made on MSH6 and γ-H2AX colocalization by counting all of the foci in at least 50 randomly chosen untreated and NCS- or IR-treated cells is given in Figure 2C and D, right panel. The analysis revealed that ~50% of MSH6 foci coincided with that of γ-H2AX 3 or 6 h after 100 ng/ml NCS or 5 Gy IR treatment, respectively. These results suggest that MSH6 may relocalize to the same DSB site as γ-H2AX after DNA damage.

MSH6 knockdown suppresses NHEJ

To investigate the biological significance of the MSH6/Ku70 interaction, we assessed the role of MSH6 in NHEJ. We combined the pEGFP–Pem1–Ad2 system and short hairpin RNA (shRNA)-mediated depletion to analyze the effects of MSH6 knockdown on the efficiency of NHEJ after formation of DSBs. The reporter cassette for detection of NHEJ activity was previously described (26). The principal characteristic of the plasmid (pEGFP–Pem1–Ad2) used in this assay (Figure 3A) is the interruption of the EGFP sequence by a 2.4-kb intron derived from the rat Pem1 gene. An exon derived from adenovirus (Ad) was introduced into the middle of the intron, and it was flanked on both sides by *Hin*dIII restriction enzyme recognition sequences. In undigested or partially digested plasmids, GFP is not expressed because the Ad exon is efficiently incorporated into the GFP mRNA. However, when the plasmid is linearized by *Hin*dIII digestion, the Ad2 exon is removed, enabling expression of EGFP upon successful intracellular recircularization. EGFP expression can then be easily detected and quantified by flow cytometry. Transfection with the supercoiled pEGFP–Pem1 plasmid is used to evaluate EGFP-signal expression without the requirement for rejoining, and the pCMV-dsRed-express plasmid is used as a control to determine transfection efficiency for this assay.

Figure 1. Continued
DNase I for 20 min at 37°C (lane 4) or mock-treated (lane 2). Cell lysates were then subjected to coimmunoprecipitation assays with MSH6 antibody and detected by anti-Ku70 or anti-MSH6. The fifth lane contains 5% input for Ku70 and 20% input for MSH6. (**E**) HeLa cells were untreated or treated with 100 ng/ml NCS, and cells were lysed at the indicated times. Whole-cell lysates were subjected to immunoprecipitation using an anti-MSH6 antibody, and the resulting immunoprecipitates were subjected to western-blot analysis using anti-Ku70 and anti-MSH6 antibodies. Graphs show the quantification of the level of Ku70. The sixth lane contains 5% input for Ku70 and 20% input for MSH6. The data were normalized to the untreated control (as the value of 1) and are the mean ± SD of three independent experiments. (**F**) HEK293T cells were transfected with full-length MSH6 and HA-tagged Ku70 expression vectors. After 24 h, cells were untreated or treated with 100 ng/ml NCS for 3 h. Proteins were immunoprecipitated from HEK293T cell lysates using an anti-MSH6 antibody, and the resulting immunoprecipitates were subjected to western-blot analysis using anti-HA or anti-MSH6 antibodies. Graphs show the quantification of the level of HA-Ku70. The third and fourth lane contains 20% input. The data were normalized to the untreated control (as the value of 1) and are the mean ± SD of three independent experiments.

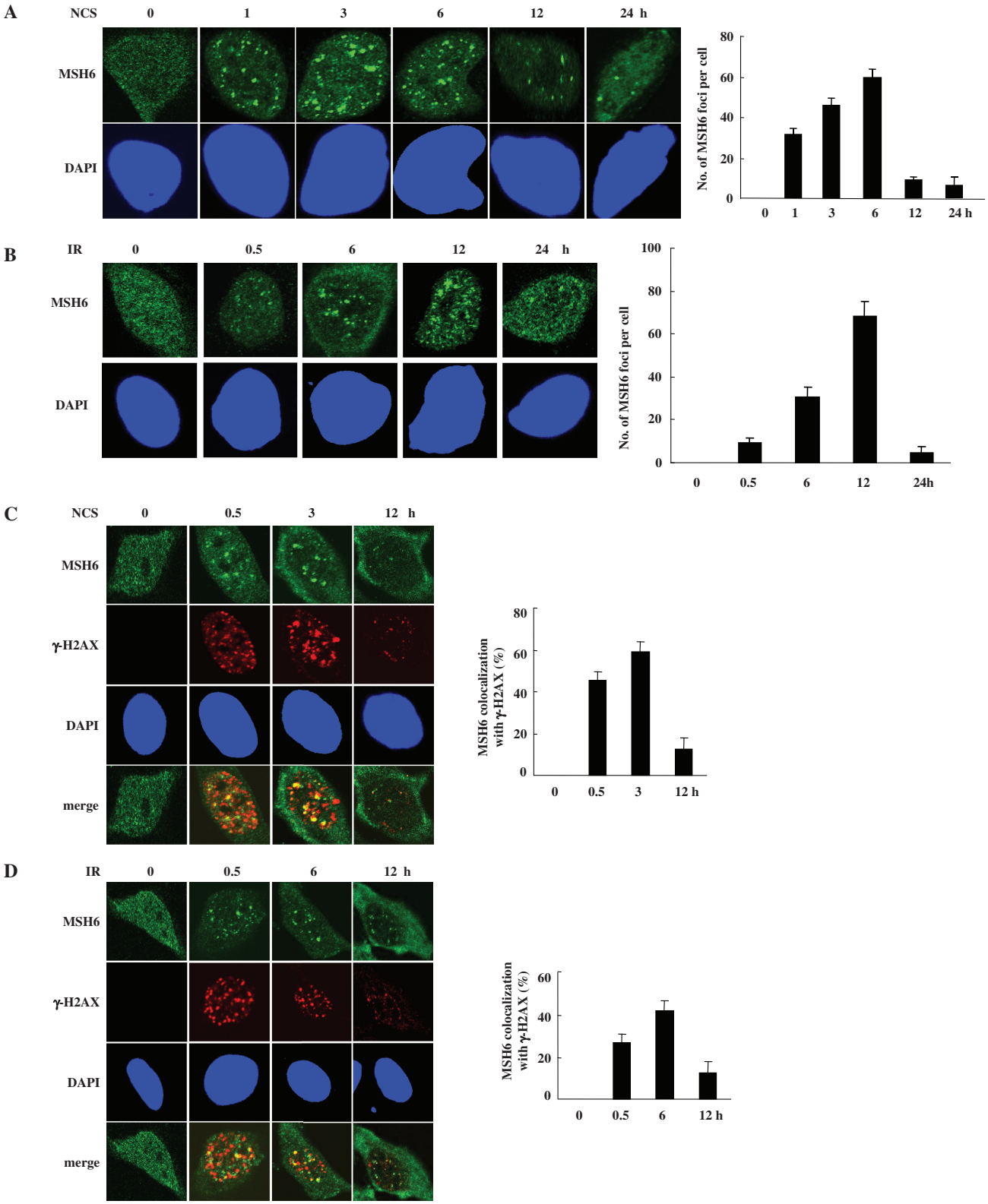

Figure 2. MSH6 forms nuclear foci that colocalize with γ-H2AX after DNA damage. (**A** and **B**) HeLa cells were untreated or treated with 100 ng/ml NCS (A) or 5 Gy ionizing radiation (IR) (B). At the indicated times, cells were fixed and immunostained using an anti-MSH6 antibody. Representative cells containing foci are shown. Nuclei were stained with DAPI. The number of MSH6 foci ('Materials and Methods' section) determined by confocal microscopy ($N = 3$). (**C** and **D**) HeLa cells were untreated (UT) or treated with 100 ng/ml NCS (C) or 5 Gy ionizing radiation (IR) (D) and fixed for the indicated time points after NCS or IR treatment. Colocalization of endogenous MSH6 and γ-H2AX was detected using antibodies specific for MSH6 and γ-H2AX. MSH6 and γ-H2AX antibodies were visualized with Alexa Fluor 488- or Alexa Fluor 546-conjugated secondary antibodies, respectively, followed by confocal microscopy. Colocalization of MSH6 (green) and Ku70 (red) in cells appears yellow in merged images. Quantification of the percentage of foci showing colocalization between MSH6 and γ-H2AX. An average of 50 merged nuclear foci from three independent slides was analyzed for each time point.

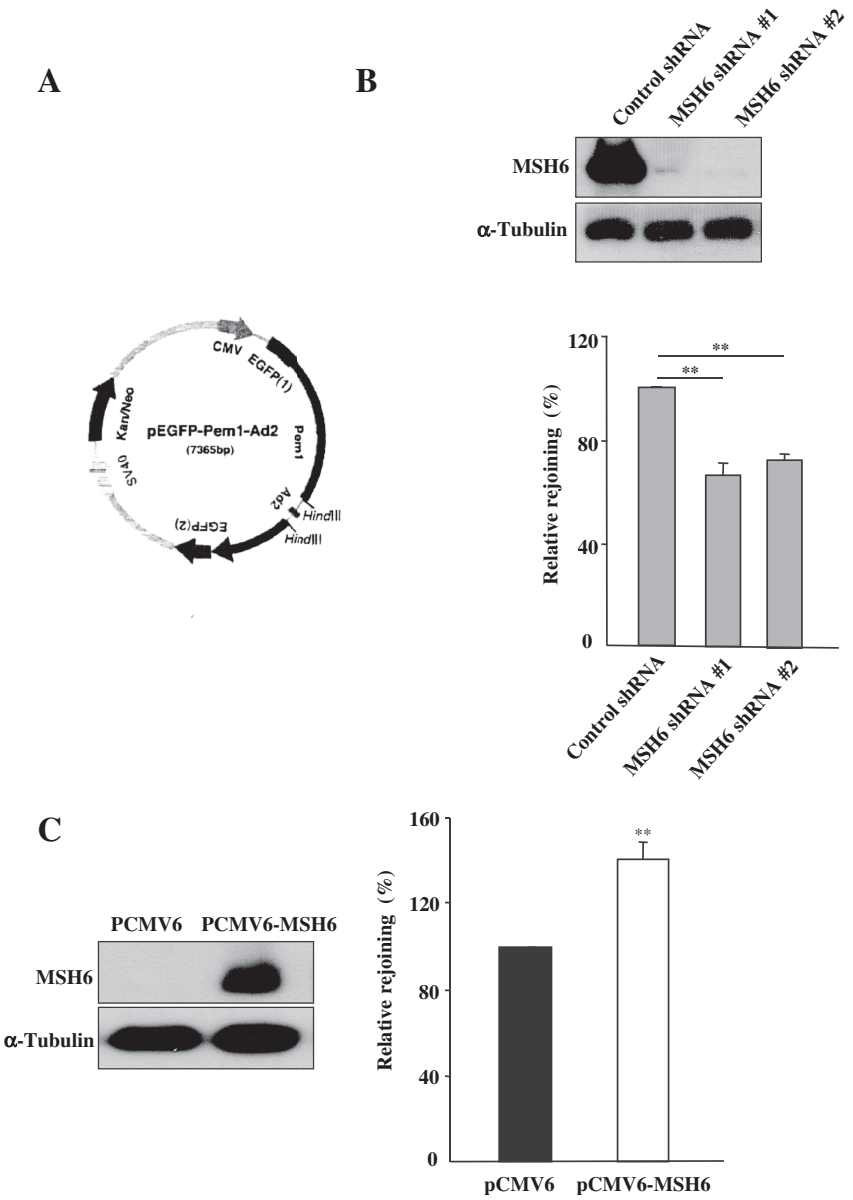

Figure 3. Effect of MSH6 on NHEJ. (**A**) Map of the pEGFP–Pem1–Ad2 vector. The reporter substrate consists of the GFP gene under control of the CMV promoter. The GFP gene contains an engineered intron from the rat Pem1 gene, which is interrupted by an adenoviral exon (Ad) that is flanked by *Hin*dIII recognition sites. In this construct, the GFP gene is inactive; however, after digestion with *Hin*dIII and successful NHEJ, the construct expresses GFP. (**B**) HeLa cells were transfected with control or one of two different MSH6 shRNA expression vectors (MSH6 shRNA #1 and #2) and selected with 400 g/ml G418. Four weeks later, the expression level of the MSH6 protein was determined by immunoblot analysis using an anti-MSH6 antibody. Control and MSH6-knockdown HeLa cells were transfected with supercoiled pEGF–Pem1 or *Hin*dIII-linearized pEGFP–Pem–Ad2 together with pCMV-dsRed-express. To quantify NHEJ events, the cells were analyzed by flow cytometry 24 h after transfection. DsRed expression was used to normalize transfection efficiency. The ratio of GFP-positive (GFP^+) to DsRed-positive ($DsRed^+$) cells was used as a measure of NHEJ. Relative levels of plasmid rejoining compared to control shRNA-transfected cells were calculated by dividing the $GFP^+/DsRed^+$ ratios of the samples and plotted. Means are representative of at least three independent experiments. Error bars indicate the SD. Asterisk denotes $P < 0.01$. (**C**) DLD1 cells were transiently transfected with either the control vector (PCMV6) or an MSH6 expression vector (pCMV6–MSH6). The level of MSH6 expression in rescued cells was analyzed by western blotting using an antibody specific for MSH6. NHEJ in control and MSH6-expressing DLD1 cells was measured using the pEGFP–Pem–Ad2 system. Means are representative of at least three independent experiments. Error bars indicate the S.D. Asterisk denotes $P < 0.01$.

To determine whether MSH6 plays a role in regulation of NHEJ activity, we first silenced MSH6 in HeLa cells using plasmid-mediated shRNA expression technology to create stable MSH6 knockdown cell lines (MSH6 shRNA #1 and MSH6 shRNA #2). Immunoblotting confirmed that expression of endogenous MSH6 was reduced by more than 90% in both cell lines stably transfected with the two different MSH6 shRNAs in comparison to control shRNA-transfected cells (Figure 3B).

To evaluate the efficiency of NHEJ, MSH6 knockdown cells (MSH6 shRNA #1 and MSH6 shRNA #2) were transfected with either linearized pEGFP–Pem1–Ad2 or

supercoiled pEGFP–Pem1 together with pDsRed2–N1. The cells were then incubated for 24 h to allow expression of EGFP (green) and DsRed (red), followed by flow cytometry analysis. To control for the efficiency of transfection, the ratio of GFP^+ cells to $DsRed^+$ cells was used as the normalized measure of NHEJ efficiency. As shown in Figure 3B, lower panel, NHEJ activity decreased significantly in both MSH6-depleted cell lines in comparison to control cells. In three independent experiments, the average NHEJ efficiency was $66.11 \pm 4.95\%$ in the MSH6 shRNA #1 cells and $72.81 \pm 2.44\%$ in the MSH6 shRNA #2 cells relative to control shRNA-transfected cells. These results indicate that MSH6 contributes to DSB repair through regulation of NHEJ.

MSH6 expression stimulates NHEJ

The reduced NHEJ activity present in cells depleted of MSH6 raised the possibility that restoration of MSH6 in MMR-deficient cells may increase NHEJ activity. To assess this possibility, we utilized the human colon cancer cell line DLD1, which is deficient for MSH6 (33). We transiently transfected DLD1 cells with the pCMV6-hMSH6 vector, which drives expression of full-length MSH6, or with the control pCMV6 vector. Western-blot analysis confirmed that MSH6 was highly expressed 24 h after transfection with the pcDNA3–MSH6 plasmid (Figure 3C, upper panel). MSH6-expressing cells were then transfected with either linearized pEGFP–Pem1–Ad2 or supercoiled pEGFP–Pem1 together with pDsRed2–N1, and the numbers of red and green fluorescent cells were quantified by FACS after 24 h. Introduction of the *Hin*dIII-linearized pEGFP–Pem1–Ad2 plasmid into MSH6-expressing DLD1 cells revealed an ~50% increase in NHEJ activity in comparison to control DLD1 cells (Figure 3C, lower panel). These results indicate that MSH6 is involved in regulation of the NHEJ pathway for repair of DSBs.

MSH6 knockdown delays DNA DSB repair

To further address whether MSH6-deficient cells exhibit defects in rejoining DNA DSBs, the formation of γ-H2AX foci was analyzed. One of the primary responses to the formation of DSBs is phosphorylation of the histone variant H2AX at Ser193 (32). Levels of phosphorylated H2AX (γ-H2AX) and quantitative analysis of γ-H2AX foci following IR are often used as measures of DSB induction and the efficiency of DNA repair. We therefore investigated whether MSH6 knockdown affected the formation of γ-H2AX foci by immunofluorescence microscopy after NCS (Figure 4A and B) or IR treatment (Figures 4C). In control cells, the maximum number of γ-H2AX foci were observed ~1 h after treatment with 100 ng/ml NCS (Figure 4B) or 5 Gy IR (Figure 4C). Longer recovery times resulted in a decline in the number of γ-H2AX foci. By 6 h after NCS or IR treatment, γ-H2AX foci were significantly decreased, indicating that the NCS- or IR-induced DSBs were almost repaired. In contrast, although the formation of γ-H2AX foci was similar in control and in MSH6-deficient cells up to 30 min after NCS or IR treatment, γ-H2AX foci persisted for longer time periods in MSH6-knockdown cells compared to control cells. MSH6-knockdown cells contained a significant amount of γ-H2AX nuclear foci even at 6 h after NCS or IR treatment.

To confirm these results, we also measured the persistence of DSB in NCS- or IR-treated HeLa cells stably transfected with MSH6 or control shRNA by single-cell electrophoresis (the comet assay). This very sensitive method can be used to detect low levels of DNA breaks. NCS or IR treatment induces DSBs, visible as increased DNA mobility or 'comet tails'. At 30 min after NCS or IR treatment, control and MSH6-knockdown cells exhibited comparable levels of DNA damage. However, when the persistence of unrepaired DNA-strand breaks was analyzed at a various times after NCS or IR treatment, cells depleted of MSH6 exhibited significantly lower repair efficiency than control cells (Figure 5A and B). Based on the comet tail moments, which quantify the extent of DNA damage, we estimate that ~2–2.5-fold more unresolved DNA damage remains in MSH6-deficient cells in comparison to control cells at 6 and 12 h after NCS or IR treatment (Figure 5A and B). These results demonstrate that MSH6 deficiency retards DNA repair of NCS-induced DNA-strand breaks.

Since radiosensitivity of cells is also affected by proteins involved in DSB repair, we monitored the survival of cells depleted of MSH6 after exposure to NCS or IR. The sensitivity of the cells to NCS or IR was examined by assaying colony formation after NCS or IR treatment. We found that inhibition of MSH6 expression reduced the number of colonies formed within 15 days after treatment with 50 and 100 ng/ml NCS (Figure 6A) or 2 and 5 Gy IR (Figure 6B). Taken together, results from our functional analyses provide clear evidence that MSH6 is involved in the efficient repair of DSBs and is required for optimal cell survival following NCS- or IR-induced DNA damage.

DISCUSSION

MMR removes DNA mismatches that have evaded proofreading during DNA replication. This versatile postreplicative repair system efficiently corrects single-base mismatches and loops of up to 16 extrahelical nucleotides that arise during replication of repetitive DNA tracts (21,34). Repair is initiated by binding of one of two mismatch recognition complexes that have overlapping specificities, ensuring efficient repair of all common replication errors. The MutSα and MutSβ mismatch recognition complexes are heterodimers of hMSH2/hMSH6 and hMSH2/hMSH3, respectively. The MutSα complex binds to and participates in the repair of single base–base mismatches and insertion/deletion loops, whereas the MutSβ complex recognizes insertion/deletion loops larger than the single-base mispairs (27,35). Another heterodimeric complex made up of hMLH and hPMS2 forms a ternary complex with the MutS complexes and promotes repair via its endonucleolytic activity, leading to excision repair of the mismatch (36).

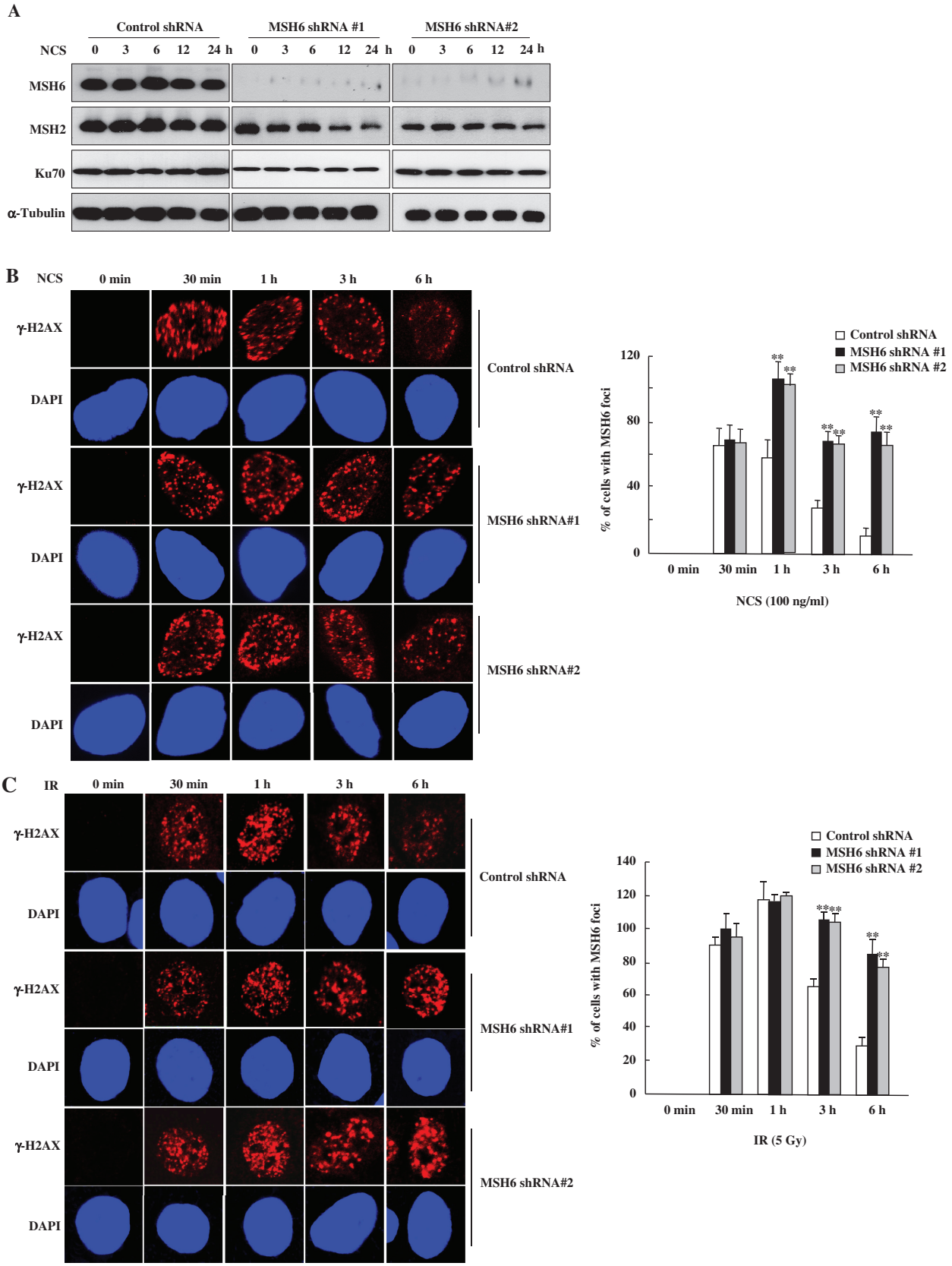

Figure 4. MSH6-deficient cells exhibit prolonged γ-H2AX staining. (**A**) Control and MSH6-depleted HeLa cells were untreated (0 min) or treated with 100 ng/ml NCS. Whole-cell lysates were prepared at the indicated time points, and western-blot analysis was performed using specific antibodies directed against MSH6, MSH2, Ku70 and α-tubulin. (**B** and **C**) Control and MSH6-depleted HeLa cells were untreated or treated with 100 ng/ml NCS (B) or 5 Gy ionizing radiation (C) and were then fixed at the indicated times. Cells were stained with an anti-γ-H2AX antibody and the DNA was counterstained using DAPI. The percentage of γ-H2AX foci positive cells determined by confocal microscopy ($N = 3$). Error bars represent the mean ± SD. Asterisk denotes $P < 0.01$.

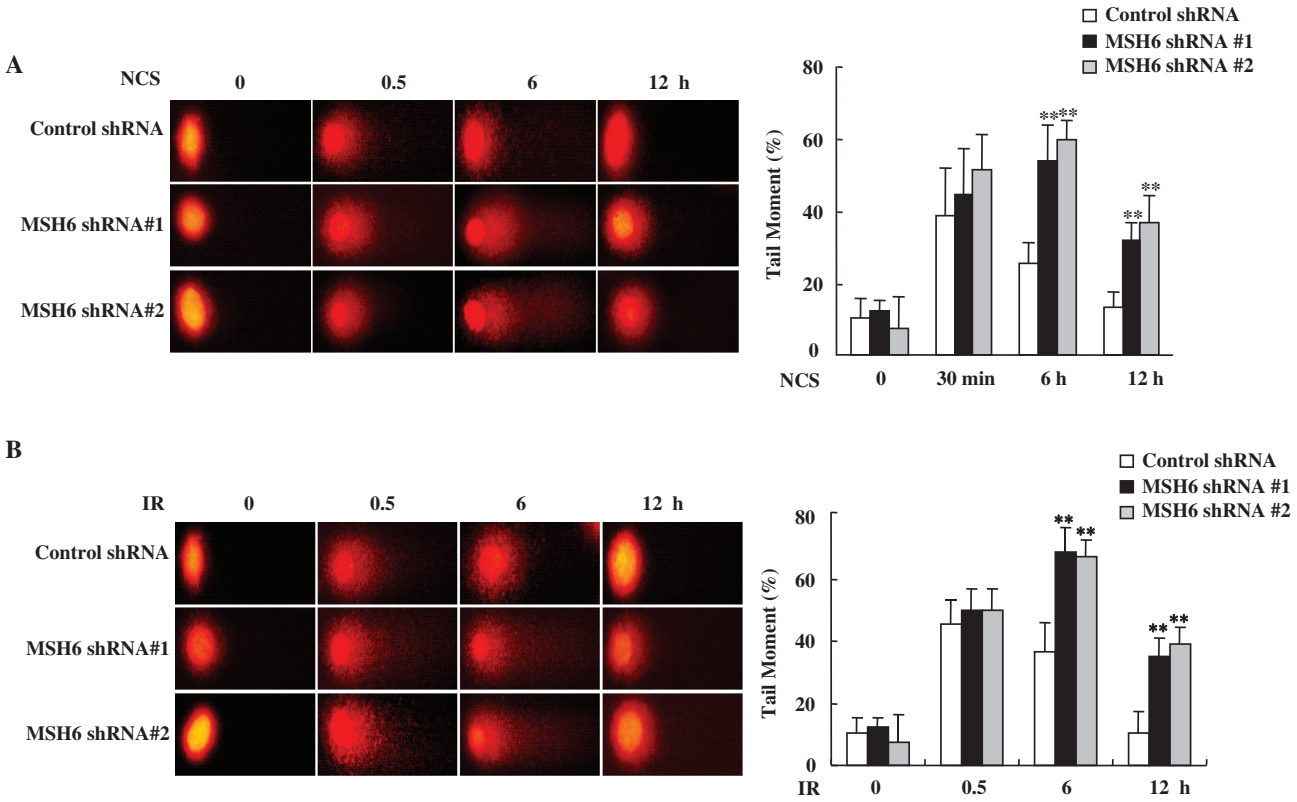

Figure 5. MSH6 knockdown results in decreased DSB repair. (**A** and **B**) Control and MSH6-depleted HeLa cells were untreated or treated with 100 ng/ml NCS (A) or 5 Gy ionizing radiation (B). At the indicated time points, cells were harvested for comet tail formation assays under alkaline conditions. Comet images were captured using fluorescence microscopy, and tail moment was analyzed in 75–80 randomly chosen comets using Komet 5.5 analysis software. Representative comet images observed at different time points after NCS treatment are shown. Changes in the percentage of relative comet tail moments between control and MSH6 knockdown cells after treatment of NCS or ionizing radiation. Histograms represent the average of three independent experiments. Error bars represent the mean ± SD. Asterisk denotes $P < 0.01$.

In addition to their functions in post-replicative MMR, MMR proteins also participate in many cellular processes through associations with DNA-damage-signaling proteins. For example, MMR proteins, including MSH2, MSH6 and MLH1, are components of the BRCA-1-associated genome surveillance complex, a multi-protein complex involved in the recognition and response to abnormal DNA structures (37). In addition, MSH2 constitutively interacts with the ATR kinase to form a signaling module that regulates phosphorylation of downstream effectors, such as Chk1 (38). MLH1 and MSH2 also act as adaptors that link ATM and Chk2 in response to DNA damage through associations with these proteins (39). PMS2 collaborates with p73 to enhance cisplatin-induced apoptosis (40). The interaction between MMR and base excision repair pathways is critical for modulating the DNA-damage response (41). The three MutL homologs, MLH1, PMS2 and PMS1, have been shown to interact with a large number of proteins involved in cell-cycle regulation, signaling and apoptosis (42). Therefore, identification of MMR-binding proteins and the functional significance of their interactions are important for understanding the myriad biological functions of these proteins.

In this study, we present several independent observations that document a specific interaction between the human MMR protein MSH6 and Ku70. First, we used yeast two-hybrid assays to show that MSH6 interacts with Ku70. Second, we found that Ku70 co-immunoprecipitates with MSH6 from HeLa cell extracts and that this interaction is enhanced after radiomimetic NCS or IR exposure. Third, MSH6 forms NCS- or IR-induced nuclear foci that colocalize with γ-H2AX at the sites of DNA breaks. Finally, we showed that the interaction between MSH6 and Ku70 regulates NHEJ activity, which is critical for repair of DSBs. These biochemical and morphological observations, as well as our functional analyses, provide compelling evidence for a nuclear complex consisting of MSH6 and Ku70.

Recently, several lines of evidence suggest that MMR plays a role in repair of DSBs (2), which can be repaired by HR (23,43–46) or NHEJ (24,25,47). However, the underlying mechanisms by which MMR regulates DSB repair remain unknown. In the present study, we showed that MSH6 is readily accumulated at the sites of DSBs, where it colocalizes with γ-H2AX after NCS or IR treatment (Figure 2C and D). Co-immunoprecipitation experiments also revealed that MSH6 associates with Ku70 within 3 h after NCS treatment and that this interaction returns to basal levels at 12 h post-NCS treatment (Figure 1E). In addition, endogenous MSH6 and Ku86 could be coimmunoprecipitated, and this was increased after treatment of NCS. On the other hand, endogenous

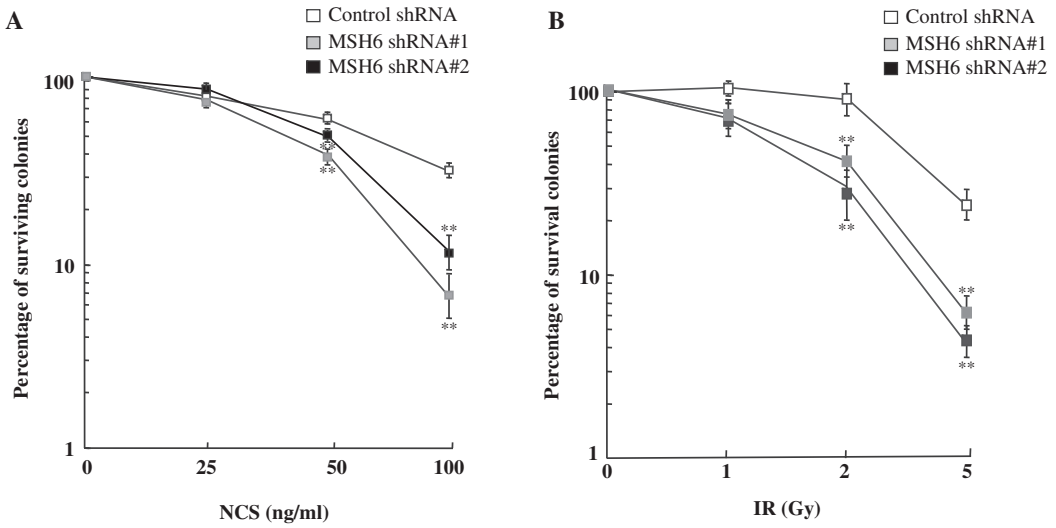

Figure 6. MSH6 depletion influences survival of HeLa cells following exposure to NCS. (**A** and **B**) Control and MSH6-knockdown HeLa cells were untreated or treated with the indicated doses of NCS (A) or ionizing radiation (B) and cell survival was assessed using a clonogenic assay. Data represent the mean ± SD of three independent experiments. Asterisk denotes $P < 0.01$.

MSH6 and endogenous DNA-PKcs did not interact in the absence of NCS, but upon NCS treatment the interaction was found (Figure 1C, third panel). However, interaction between MSH6 and XRCC4 in the presence of NCS was not detected by coimmunoprecipitation (Figure 1C, fourth panel). Together, these data suggest that MSH6 may relocalize to the DSB site following NCS or IR treatment and work co-orporately Ku70 and play a role in early process of NHEJ in response to DNA damage.

Therefore, we next further explored whether MSH6 is involved in the repair of DSBs. We utilized MSH6-deficient human HeLa cells to investigate whether MSH6 knockdown affected DSB repair using two different assays that measure the levels of DSBs in cells exposed to survival curve range doses of NCS, the γ-H2AX and comet assays. An early step in the cellular response to DSBs is phosphorylation of the histone variant H2AX (32). Numbers of γ-H2AX foci have been shown to correlate with DNA damage levels measured by single-cell electrophoresis, an established method used to determine numbers of DSBs. Using γ-H2AX foci analysis as an approach to measure DSB repair, we compared repair in MSH6-knockdown cells and control cells treated with the radiomimetic drug NCS. Our results showed that MSH6-deficient HeLa cells have a significant repair defect that was detected both by γ-H2AX foci and comet tail analyses. The initial levels of DSBs after NCS or IR treatment were similar in the two MSH6 knockdown cell lines (MSH6 shRNA #1 and #2) and in the control cells (control shRNA) (30 min; Figure 4B and C). However, both MSH6 knockdown cell lines exhibited significant levels of unrejoined DSBs at 1 h after exposure to NCS. Importantly, although control cells had almost normal levels of γ-H2AX foci 3 h after NCS treatment, disappearance of γ-H2AX foci in MSH6-deficient cells was significantly delayed. Similar results were also obtained by control and MSH6 knockdown cells exposed to IR. Comet assay data shown in Figure 5 also indicate that rejoining of NCS- or IR-induced DSBs was significantly delayed by MSH6 knockdown, similar to γ-H2AX foci measurements. These findings support a role for MSH6 in DSB repair in human cells.

NHEJ was previously reported to be decreased in MMR-deficient colon cancer cell lines in comparison to MMR-proficient cells (47). Since inactivating mutations frequently occur in the hRAD50 and hMRE11 genes in MMR-deficient tumors (47–49), impaired expression of these proteins has been suggested to lead to decreased MRE11/RAD50/NBS1 complex formation, decreased NHEJ and increased sensitivity to IR. However, the MMR-deficient colon cancer cell line DLD1, which contains a mutation in the MSH6 gene (33), has normal hRAD50 and hMRE11 expression but still exhibits decreased NHEJ activity in comparison to MSH6-proficient cells (47). As described above, we demonstrated that MSH6 interacts with Ku70 and that HeLa cells stably expressing MSH6 shRNAs exhibit impaired ability to repair DSBs. Thus, it seems reasonable to expect that MSH6 contributes directly to NHEJ activity. Using an *in vivo* repair assay that makes use of plasmids linearized with *Hin*dIII to generate non-complementary ends, we provided direct evidence that MSH6 promotes DSB-induced NHEJ. MSH6-deficient HeLa cells were shown to exhibit an ∼30% reduction in *Hin*dIII-induced NHEJ (Figure 3B). We further confirmed the effects of MSH6 on *Hin*dIII-induced NHEJ in DLD1 cells rescued with MSH6. We found that the overexpression of MSH6 in DLD1 cells increases NHEJ activity (Figure 3C). In contrast to our findings, Jacob *et al.* (50) reported that the ability to perform efficient end joining did not require a functional-MMR system, as no significant differences were observed in the rejoining efficiency of NHEJ between DLD1 and DLD1-Ch2 cells containing chromosome 2, which includes wild-type hMSH6. The

discrepancy between our results and the findings of the previous study could be due to differing expression levels of MSH6 between DLD1-ch2 cells and MSH6-overexpressing DLD1 cells or due to different methods of *in vivo* rejoining. Thus, further evaluation is needed to better characterize the changes in efficiency of NHEJ in cells with different levels of MSH6 using several different methods.

Cell lines defective for any of the DSB repair genes are generally highly sensitive to IR and have marked deficiencies in DSB repair (51). Knockout or knockdown of Ku70 (52,53) or DNA-PK_{CS} (54) has been shown to result in hypersensitivity to radiation. Loss of MMR activity generally renders cells less sensitive to cell killing by DNA-damaging agents, reflecting the role(s) of the MMR system in DNA-damage signaling used to trigger cell-cycle arrest and apoptosis (55,56). However, our data indicate that MSH6-knockdown cells are significantly more sensitive to NCS and IR than control cells (Figure 6). A similar increased sensitivity to γ-irradiation and the DNA DSB-producing drug, bleomycin, has also been reported for MMR-deficient cell lines (47,57). In the HeLa and DLD1 cell studies described above, cells depleted of MSH6 exhibited impaired DSB rejoining and NHEJ, and ectopic expression of MSH6 in deficient cells restored NHEJ activity. Hence, loss of MSH6-mediated NHEJ activation likely permits cells with broken DNA to enter mitosis, resulting in mitotic catastrophe.

Although this is the first report demonstrating that MSH6 regulates MHEJ activity, many questions remain regarding how NHEJ is actually regulated by the MSH6. The NHEJ process is initiated by binding the Ku70/80 heterodimer to both ends of the broken-DNA molecule. Binding of Ku to DNA is a critical step that creates a scaffold for the assembly of the other key enzymes necessary for NHEJ (58). The X-ray crystal structure of Ku shows that it binds to DNA via a channel generated by heterodimer formation (59). Thus, the MSH6 could further increase the binding affinity of Ku for DNA, modulate the amount of Ku70/80 heterodimer complexes or facilitate the recruitment of other important NHEJ proteins to bind the broken-DNA ends. Accordingly, studies aimed at determining the detailed mechanisms underlying MSH6 modulation of NHEJ efficiency are currently under way.

SUPPLEMENTARY DATA

Supplementary Data are available at NAR Online.

FUNDING

Funding for open access charge: Ministry of Education, Science and Technology, the Korean government (grants 2010-0002099 and 2009-0081796); Institute of Medical Science, Chosun University, 2009 (to I.-Y.C.).

Conflict of interest statement. None declared.

REFERENCES

1. Khanna,K.K. and Jackson,S.P. (2001) DNA double-strand breaks: signaling, repair and the cancer connection. *Nat. Genet.*, **27**, 247–254.
2. Zhang,Y., Rohde,L.H. and Wu,H. (2009) Involvement of nucleotide excision and mismatch repair mechanisms in double strand break repair. *Curr. Genomics*, **10**, 250–258.
3. Lees-Miller,S.P. and Meek,K. (2003) Repair of DNA double strand breaks by non-homologous end joining. *Biochimie*, **85**, 1161–1173.
4. Lieber,M.R., Ma,Y., Pannicke,U. and Schwarz,K. (2003) Mechanism and regulation of human non-homologous DNA end-joining. *Nat. Rev. Mol. Cell Biol.*, **4**, 712–720.
5. Downs,J.A. and Jackson,S.P. (2004) A means to a DNA end: the many roles of Ku. *Nat. Rev. Mol. Cell Biol.*, **5**, 367–378.
6. Burma,S., Chen,B.P. and Chen,D.J. (2006) Role of non-homologous end joining (NHEJ) in maintaining genomic integrity. *DNA Repair (Amst)*, **5**, 1042–1048.
7. Mimori,T., Hardin,J.A. and Steitz,J.A. (1986) Characterization of the DNA-binding protein antigen Ku recognized by autoantibodies from patients with rheumatic disorders. *J. Biol. Chem.*, **261**, 2274–2278.
8. Koike,M., Shiomi,T. and Koike,A. (2001) Dimerization and nuclear localization of ku proteins. *J. Biol. Chem.*, **276**, 11167–11173.
9. Tuteja,R. and Tuteja,N. (2000) Ku autoantigen: a multifunctional DNA-binding protein. *Crit. Rev. Biochem. Mol. Biol.*, **35**, 1–33.
10. Nolens,G., Pignon,J.C., Koopmansch,B., Elmoualij,B., Zorzi,W., De Pauw,E. and Winkler,R. (2009) Ku proteins interact with activator protein-2 transcription factors and contribute to ERBB2 overexpression in breast cancer cell lines. *Breast Cancer Res.*, **11**, R83.
11. Yin,H. and Glass,J. (2006) In prostate cancer cells the interaction of C/EBPalpha with Ku70, Ku80, and poly(ADP-ribose) polymerase-1 increases sensitivity to DNA damage. *J. Biol. Chem.*, **281**, 11496–11505.
12. Amsel,A.D., Rathaus,M., Kronman,N. and Cohen,H.Y. (2008) Regulation of the proapoptotic factor Bax by Ku70-dependent deubiquitylation. *Proc. Natl Acad. Sci. USA*, **105**, 5117–5122.
13. Ting,N.S., Yu,Y., Pohorelic,B., Lees-Miller,S.P. and Beattie,T.L. (2005) Human Ku70/80 interacts directly with hTR, the RNA component of human telomerase. *Nucleic Acids Res.*, **33**, 2090–2098.
14. Chai,W., Ford,L.P., Lenertz,L., Wright,W.E. and Shay,J.W. (2002) Human Ku70/80 associates physically with telomerase through interaction with hTERT. *J. Biol. Chem.*, **277**, 47242–47247.
15. Cohen,H.Y., Lavu,S., Bitterman,K.J., Hekking,B., Imahiyerobo,T.A., Miller,C., Frye,R., Ploegh,H., Kessler,B.M. and Sinclair,D.A. (2004) Acetylation of the C terminus of Ku70 by CBP and PCAF controls Bax-mediated apoptosis. *Mol. Cell*, **13**, 627–638.
16. Mazumder,S., Plesca,D., Kinter,M. and Almasan,A. (2007) Interaction of a cyclin E fragment with Ku70 regulates Bax-mediated apoptosis. *Mol. Cell Biol.*, **27**, 3511–3520.
17. Tanaka,Y., Imamura,J., Kanai,F., Ichimura,T., Isobe,T., Koike,M., Kudo,Y., Tateishi,K., Ikenoue,T., Ijichi,H. *et al.* (2007) Runx3 interacts with DNA repair protein Ku70. *Exp. Cell Res.*, **313**, 3251–3260.
18. Li,B. and Comai,L. (2000) Functional interaction between Ku and the werner syndrome protein in DNA end processing. *J. Biol. Chem.*, **275**, 28349–28352.
19. Karmakar,P., Snowden,C.M., Ramsden,D.A. and Bohr,V.A. (2002) Ku heterodimer binds to both ends of the Werner protein and functional interaction occurs at the Werner N-terminus. *Nucleic Acids Res.*, **30**, 3583–3591.
20. Fang,L., Wang,Y., Du,D., Yang,G., Tak Kwok,T., Kai Kong,S., Chen,B., Chen,D.J. and Chen,Z. (2007) Cell polarity protein Par3 complexes with DNA-PK via Ku70 and regulates DNA double-strand break repair. *Cell Res.*, **17**, 100–116.
21. Harfe,B.D. and Jinks-Robertson,S. (2000) DNA mismatch repair and genetic instability. *Annu. Rev. Genet.*, **34**, 359–399.

22. Sugawara,N., Paques,F., Colaiacovo,M. and Haber,J.E. (1997) Role of Saccharomyces cerevisiae Msh2 and Msh3 repair proteins in double-strand break-induced recombination. *Proc. Natl Acad. Sci. USA*, **94**, 9214–9219.
23. Elliott,B. and Jasin,M. (2001) Repair of double-strand breaks by homologous recombination in mismatch repair-defective mammalian cells. *Mol. Cell Biol.*, **21**, 2671–2682.
24. Bannister,L.A., Waldman,B.C. and Waldman,A.S. (2004) Modulation of error-prone double-strand break repair in mammalian chromosomes by DNA mismatch repair protein Mlh1. *DNA Repair (Amst)*, **3**, 465–474.
25. Smith,J.A., Waldman,B.C. and Waldman,A.S. (2005) A role for DNA mismatch repair protein Msh2 in error-prone double-strand-break repair in mammalian chromosomes. *Genetics*, **170**, 355–363.
26. Kang,Y., Lee,J.H., Hoan,N.N., Sohn,H.M., Chang,I.Y. and You,H.J. (2009) Protein phosphatase 5 regulates the function of 53BP1 after neocarzinostatin-induced DNA damage. *J. Biol. Chem.*, **284**, 9845–9853.
27. Gradia,S., Acharya,S. and Fishel,R. (1997) The human mismatch recognition complex hMSH2-hMSH6 functions as a novel molecular switch. *Cell*, **91**, 995–1005.
28. Collis,S.J., DeWeese,T.L., Jeggo,P.A. and Parker,A.R. (2005) The life and death of DNA-PK. *Oncogene*, **24**, 949–961.
29. Li,Z., Otevrel,T., Gao,Y., Cheng,H.L., Seed,B., Stamato,T.D., Taccioli,G.E. and Alt,F.W. (1995) The XRCC4 gene encodes a novel protein involved in DNA double-strand break repair and V(D)J recombination. *Cell*, **83**, 1079–1089.
30. Grawunder,U., Zimmer,D., Fugmann,S., Schwarz,K. and Lieber,M.R. (1998) DNA ligase IV is essential for V(D)J recombination and DNA double-strand break repair in human precursor lymphocytes. *Mol. Cell*, **2**, 477–484.
31. Stewart,G.S., Wang,B., Bignell,C.R., Taylor,A.M. and Elledge,S.J. (2003) MDC1 is a mediator of the mammalian DNA damage checkpoint. *Nature*, **421**, 961–966.
32. Rogakou,E.P., Pilch,D.R., Orr,A.H., Ivanova,V.S. and Bonner,W.M. (1998) DNA double-stranded breaks induce histone H2AX phosphorylation on serine 139. *J. Biol. Chem.*, **273**, 5858–5868.
33. Papadopoulos,N., Nicolaides,N.C., Liu,B., Parsons,R., Lengauer,C., Palombo,F., D'Arrigo,A., Markowitz,S., Willson,J.K., Kinzler,K.W. *et al.* (1995) Mutations of GTBP in genetically unstable cells. *Science*, **268**, 1915–1917.
34. Jiricny,J. (2006) The multifaceted mismatch-repair system. *Nat. Rev. Mol. Cell Biol.*, **7**, 335–346.
35. Genschel,J., Littman,S.J., Drummond,J.T. and Modrich,P. (1998) Isolation of MutSbeta from human cells and comparison of the mismatch repair specificities of MutSbeta and MutSalpha. *J. Biol. Chem.*, **273**, 19895–19901.
36. Kadyrov,F.A., Dzantiev,L., Constantin,N. and Modrich,P. (2006) Endonucleolytic function of MutLalpha in human mismatch repair. *Cell*, **126**, 297–308.
37. Wang,Y., Cortez,D., Yazdi,P., Neff,N., Elledge,S.J. and Qin,J. (2000) BASC, a super complex of BRCA1-associated proteins involved in the recognition and repair of aberrant DNA structures. *Genes Dev.*, **14**, 927–939.
38. Wang,Y. and Qin,J. (2003) MSH2 and ATR form a signaling module and regulate two branches of the damage response to DNA methylation. *Proc. Natl Acad. Sci. USA*, **100**, 15387–15392.
39. Brown,K.D., Rathi,A., Kamath,R., Beardsley,D.I., Zhan,Q., Mannino,J.L. and Baskaran,R. (2003) The mismatch repair system is required for S-phase checkpoint activation. *Nat. Genet.*, **33**, 80–84.
40. Shimodaira,H., Yoshioka-Yamashita,A., Kolodner,R.D. and Wang,J.Y. (2003) Interaction of mismatch repair protein PMS2 and the p53-related transcription factor p73 in apoptosis response to cisplatin. *Proc. Natl Acad. Sci. USA*, **100**, 2420–2425.
41. Kovtun,I.V. and McMurray,C.T. (2007) Crosstalk of DNA glycosylases with pathways other than base excision repair. *DNA Repair (Amst)*, **6**, 517–529.
42. Cannavo,E., Gerrits,B., Marra,G., Schlapbach,R. and Jiricny,J. (2007) Characterization of the interactome of the human MutL homologues MLH1, PMS1, and PMS2. *J. Biol. Chem.*, **282**, 2976–2986.
43. Villemure,J.F., Abaji,C., Cousineau,I. and Belmaaza,A. (2003) MSH2-deficient human cells exhibit a defect in the accurate termination of homology-directed repair of DNA double-strand breaks. *Cancer Res.*, **63**, 3334–3339.
44. Pichierri,P., Franchitto,A., Piergentili,R., Colussi,C. and Palitti,F. (2001) Hypersensitivity to camptothecin in MSH2 deficient cells is correlated with a role for MSH2 protein in recombinational repair. *Carcinogenesis*, **22**, 1781–1787.
45. Franchitto,A., Pichierri,P., Piergentili,R., Crescenzi,M., Bignami,M. and Palitti,F. (2003) The mammalian mismatch repair protein MSH2 is required for correct MRE11 and RAD51 relocalization and for efficient cell cycle arrest induced by ionizing radiation in G2 phase. *Oncogene*, **22**, 2110–2120.
46. Hong,Z., Jiang,J., Hashiguchi,K., Hoshi,M., Lan,L. and Yasui,A. (2008) Recruitment of mismatch repair proteins to the site of DNA damage in human cells. *J. Cell Sci.*, **121**, 3146–3154.
47. Koh,K.H., Kang,H.J., Li,L.S., Kim,N.G., You,K.T., Yang,E., Kim,H., Kim,H.J., Yun,C.O. and Kim,K.S. (2005) Impaired nonhomologous end-joining in mismatch repair-deficient colon carcinomas. *Lab. Invest.*, **85**, 1130–1138.
48. Kim,N.G., Choi,Y.R., Baek,M.J., Kim,Y.H., Kang,H., Kim,N.K., Min,J.S. and Kim,H. (2001) Frameshift mutations at coding mononucleotide repeats of the hRAD50 gene in gastrointestinal carcinomas with microsatellite instability. *Cancer Res.*, **61**, 36–38.
49. Giannini,G., Ristori,E., Cerignoli,F., Rinaldi,C., Zani,M., Viel,A., Ottini,L., Crescenzi,M., Martinotti,S., Bignami,M. *et al.* (2002) Human MRE11 is inactivated in mismatch repair-deficient cancers. *EMBO Rep.*, **3**, 248–254.
50. Jacob,S., Miquel,C., Sarasin,A. and Praz,F. (2005) Effects of camptothecin on double-strand break repair by non-homologous end-joining in DNA mismatch repair-deficient human colorectal cancer cell lines. *Nucleic Acids Res.*, **33**, 106–113.
51. Chang,C., Biedermann,K.A., Mezzina,M. and Brown,J.M. (1993) Characterization of the DNA double strand break repair defect in scid mice. *Cancer Res.*, **53**, 1244–1248.
52. Omori,S., Takiguchi,Y., Suda,A., Sugimoto,T., Miyazawa,H., Tanabe,N., Tatsumi,K., Kimura,H., Pardington,P.E., Chen,F. *et al.* (2002) Suppression of a DNA double-strand break repair gene, Ku70, increases radio- and chemosensitivity in a human lung carcinoma cell line. *DNA Repair (Amst)*, **1**, 299–310.
53. Ayene,I.S., Ford,L.P. and Koch,C.J. (2005) Ku protein targeting by Ku70 small interfering RNA enhances human cancer cell response to topoisomerase II inhibitor and gamma radiation. *Mol. Cancer Ther.*, **4**, 529–536.
54. Peng,Y., Zhang,Q., Nagasawa,H., Okayasu,R., Liber,H.L. and Bedford,J.S. (2002) Silencing expression of the catalytic subunit of DNA-dependent protein kinase by small interfering RNA sensitizes human cells for radiation-induced chromosome damage, cell killing, and mutation. *Cancer Res.*, **62**, 6400–6404.
55. Meyers,M., Hwang,A., Wagner,M.W. and Boothman,D.A. (2004) Role of DNA mismatch repair in apoptotic responses to therapeutic agents. *Environ. Mol. Mutagen.*, **44**, 249–264.
56. Stojic,L., Brun,R. and Jiricny,J. (2004) Mismatch repair and DNA damage signalling. *DNA Repair (Amst)*, **3**, 1091–1101.
57. Li,H.R., Shagisultanova,E.I., Yamashita,K., Piao,Z., Perucho,M. and Malkhosyan,S.R. (2004) Hypersensitivity of tumor cell lines with microsatellite instability to DNA double strand break producing chemotherapeutic agent bleomycin. *Cancer Res.*, **64**, 4760–4767.
58. Weterings,E. and Chen,D.J. (2008) The endless tale of non-homologous end-joining. *Cell Res.*, **18**, 114–124.
59. Walker,J.R., Corpina,R.A. and Goldberg,J. (2001) Structure of the Ku heterodimer bound to DNA and its implications for double-strand break repair. *Nature*, **412**, 607–614.